Jarchlo, Elnaz Alizadeh ; Tang, Xuan; Doroud, Hossein; Gil Jiménez, Víctor P.; Lin, Bangjiang; Casari, Paolo; Ghassemlooy, Zabih. (2019). Li-Tect: 3D Monitoring and Shape Detection using Visible Light Sensors. *IEEE Sensors Journal*, 19(3), pp.: 940-949.

DOI: https://doi.org/10.1109/JSEN.2018.2879398

Li-Tect: 3D Monitoring and Shape Detection using Visible Light Sensors

Elnaz Alizadeh Jarchlo, Xuan Tang, Hossein Doroud, Victor P. Gil Jimenez, Bangjiang Lin, Paolo Casari, Zabih Ghassemlooy

***Abstract*—In this paper, we propose Li-Tect, an algorithm to detect the shape of an object located in an indoor environment using low cost optical elements through sensing the environment's light. The algorithm analyzes, relying on the predictability of optical propagation paths, how much light is expected to propagate in the absence of obstructions caused by the presence of an object. Then, based on the received light when the object is in the room, the algorithm infers the shape of the object. In addition, the algorithm considers the reflected paths from surfaces in order to determine the object's estimated shape. We study five different scenarios characterized by different levels of complexity, room sizes and a range of reflection nodes. The algorithm is also tested in a real prototype where several experiments are carried out in two scenarios to demonstrate the capabilities of Li-Tect in two and three dimensional monitoring and shape detection cases. Finally, the results show that the shape and the detection of objects in the scenarios can be easily acquired with high accuracy, even if the number of transceivers is reduced.**

***Index Terms*—Ray Tracing, Monitoring, Visible Light Sensors, Shape Detection, Visible Light Communications**

I. Introduction

VISIBLE Light Communications (VLC), which uses the visible spectrum between 375 and 780 nm, refers to the intensity modulating of the solid state based lighting fixtures i.e., light emitting diodes (LEDs) used for illuminations [1]. Considering the sufficiently high rate of modulation, flickering is undetectable by the human eyes [2]. The potential of VLC is being explored for a number of applications including high-speed (i.e., beyond the trade-mark level of Gbps) data communications in indoor environments, vehicular networks [3], airplane cabins [4], trains [5] and intelligent traffic lights management [6], [7], indoor positioning [8], motion detection [9], occupancy detection [10], ranging and detection [11] among others. However, to fully and effectively be able to adopt and implement the VLC technology in real environments there are still a number of challenges, which need to be addressed, including the physical layer (higher data rates versus the transmission span), interference management [12], medium access control (MAC) [13], integration with existing optical fiber and radio frequency wireless systems, mobility [14], shadowing [15] or peak-to-average-power ratio [16].

In addition to data transmission, VLC can be used for highly accurate indoor localization, mobility prediction, sensing and shape detection. Since lighting fixtures are pervasive, they can be used for accurate monitoring of people, and objects in indoor environments as part of smart homes [17]. Thus, no the need for installation of other specialized equipment such as motion detection sensors and cameras with high accuracy and quality. In fact, the cameras could be effectively utilized for vision, data communications and shape detection [18], but at high cost and with loss in privacy because cameras record many unnecessary details such as gender, age or clothing which might be not pleasant to end users. Besides, VLC is inherently more secure than other wireless communications. This is due to the light being confined within a room and therefore, access is only possible by being within the illumination range. Thus, the visible light sensors (VLS) are more cost and energy efficient than other sensors (i.e., motion sensor, cameras, etc.) As it is foreseen, the smart VLC-enabled lighting will become pervasive in the future and they can be utilized as VLSs. In this paper, we propose to rely on the smart lighting infrastructure for high-resolution sensing tasks. More specifically, we design, implement and evaluate both by simulations and experimental measurements the proposed monitoring and shape detection algorithm, which is denoted as Li-Tect. Li-Tect leverages on the information obtained from both active and in-active links of the spatially distributed VLS. The proposed algorithm uses only VLSs with no requirement for additional equipment such as a camera or motion sensors. VLS can be used for monitoring elderly people and patients at homes or hospitals, where it can be mounted on the door frames, beds, bathroom and etc.

The remainder of this paper is organized as follows: Section II briefly overviews related approaches for shape detection using light and RF techniques. Section III presents the proposed monitoring and shape detection algorithm. Section IV presents the simulation results and Section V demonstrates the implementation of the algorithm in real-world case studies. Finally, Section VI concludes the paper.

II. Related work

Different approaches have been proposed to detect the presence of an object within an indoor environment. They are mainly based on the RF technology (e.g., WiFi or ZigBee), but more recently the focus has been moved to VLC for object detection. We first give an overview of a VLC system, and conclude by surveying other non-light based shape detection schemes.

A. LiSense

The LiSense system [19] enables data communications and fine-grained human skeleton reconstruction in real time using the VLC technology. LiSense works based on the shadows that a human body projects on the floor in an indoor environment

by blocking the light emitted by a set of LED-based beacons. The system separates light rays from each LED source and detects shadowed sections on the floor of an indoor area thanks to deploy of photodiodes. The shadow-based information is used to reconstruct the user's 3D skeleton in order to determine the user's posture and gestures. The main issues with in LiSense are: (i) the need for a large number of PDs positioned on the floor for capturing detailed shadow based information; (ii) the assumption made that the blocking is mainly due the people not objects within a room; and (iii) not scalable since it works only for a single user with a known location and orientation with each LED flashing at a unique frequency.

B. StarLight

StarLight [20] continuously tracks the human skeleton posture by using LED panels installed on the ceiling in order to generate homogeneous light, and uses PDs to detect light blockage. Additionally, LEDs located on the floor could be used to define together a virtual shadow map, which can be projected on to the ceiling. With PDs positioned at different locations, virtual shadow maps from different viewing angles are used together to reconstruct the skeleton of a mobile user starting from the coarse body features. The output of the algorithm includes the user's current location based on the estimated features and trajectories of the environment. To avoid different LED beacons interfering, StarLight organizes transmission into a time-frequency frame, where simultaneous transmission is achieved using different frequencies. It requires a close control of the light deployment topology, and is sensitive to vertical movements, which can have a critical impact on the accuracy of the shape detection algorithm.

C. Other shape detection techniques

There are other schemes for detection of the human figure and posture. In [21] the concept of RF-Capture was introduced to detect the presence of human through a wall using the RF signals. This system can distinguish various users with different body shapes. Short and long-term averaged variance ratio (SVR and LVR, respectively) concepts are two passive WiFi-based schemes that are used to detect human motion in real-time [22]. Note that, in these schemes the phases of WiFi signals are particularly sensitive to slow human motion. In [23] processing of changes in the received signal strength indicator (RSSI) for 2.4-GHz wireless power outlets were used for sensor-less detection of human presence.
Li-Tect offers an improved shape and posture detection method where there is no requirement for precise shadow estimation, thereby avoiding complexity due to shadow overlapping and blurry shadow edges. Moreover, the proposed Li-Tect can achieve a reasonable accuracy with fewer sensors, thus saving additional lighting infrastructure for cases where a high shape detection accuracy is sought. The next section describes the algorithm in detail.

III. LI-TECT CONCEPT

The Li-Tect algorithm works by assuming that a number of smart VLSs is deployed in an indoor environment, which are aware of their locations and have information on the other sensor to establish communications. In the most basic version of Li-Tect communications between VLSs are via the line-of-sight (LoS). Thus, a VLS is a LED or PD which positions are known. Since light does not propagate through walls, the security level of algorithm is high at the physical layer. The general idea behind Li-Tect is to detect which light propagation paths are blocked by an object. Next, the shape of the object is inferred by comparing the missing links against the remaining active paths. To achieve this, the ray tracing algorithm is used for modeling the propagation paths between two VLSs. This allows to infer the path of the surviving rays with the presence of a blocking object, and therefore be able to estimate the shape of the object. These two steps are described separately in the two following subsections.

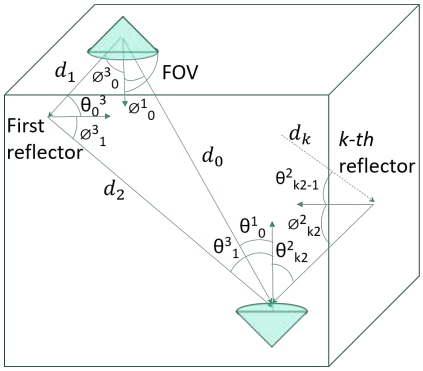

Fig. 1: Geometry of a multipath VLC channel.

A. Ray tracing

The first step in Li-Tect algorithm is to trace rays emitted by LEDs and predict their destination via LoS and reflected paths. It should be noted that diffuse configuration is not considered here, but could be part of the future work. Regarding the propagation of VLC signal, the model in [24] is used, that is summarized below. Fig. 1 shows a single transmitter (Tx) with an effective transmission area A_{eff} and a single receiver (Rx) with an effective reception area A_{PD}, and both LoS and non-LoS paths. The channel impulse response is given as

$$\sum_{r=1}^{N_r} h^{k_r}(t;\mathbf{\Phi}^r)\,, \tag{1}$$

where N_r is the number of transmitted rays that reach the Rx, k_r is the number of reflections incurred by the rth ray, and $\mathbf{\Phi}^r = [\phi_0^r, \ldots, \phi_{k_r}^r]^T$ is the vector containing the transmission (ϕ_0^r) and reflection ($\phi_1^r, \ldots, \phi_{k_r}^r$) angles of a ray. Each term of 1) can be calculated as [24]:

$$h^{k_r}(t;\mathbf{\Phi}^r) = \int_S L_0^r \ldots L_{k_r}^r \Gamma^{k_r} \mathbb{1}\left[\frac{\theta_{k_r}}{FoV}\right] \delta\left(t - \frac{d_0 + \ldots + d_k}{c}\right) \mathrm{d}A \tag{2}$$

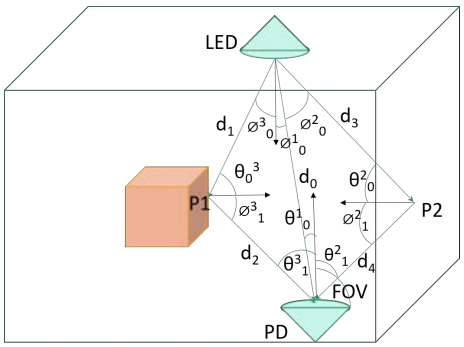

- P1: Reflection point on the Object
- P2: Reflection point on the wall

Fig. 2: Geometry of a multipath VLC channel with an object.

where θ_i is the arrival angle of the ith reflection, and

$$L_1^r = \frac{A_{eff}(m+1)\cos^m\phi_0^r\cos\theta_0^r}{2\pi d_0^2}, \quad L_2^r = \frac{\cos\phi_1^r cos\theta_1^r}{\pi d_1^2}, \ldots$$
$$L_{k_r}^r = \frac{A_{PD}\cos\phi_{k_r}^r cos\theta_{k_r}^r}{\pi d_{k_r}^2} \tag{3}$$

where $m = -1/(\log_2\cos\phi_{1/2})$, is the mode number of the LED's radiation pattern, $FoV = 2\phi_{1/2}$ is the field of view of the LED, d_i is the distance traveled by a ray before the ith reflection, and $\mathbb{1}[x] = 1$ if $|x| \leq 1$, and 0 otherwise, implying that an Rx can detect a ray only if its angle of arrival is within the Rx's FoV. The Γ^{k_r} denotes the power of the ray after k_r bounces, and is approximated to $\Gamma^{k_r} = P_r\bar{\rho}_1\cdots\bar{\rho}_{k_r}$ as in [24], where $\bar{\rho}_i$ is the average reflectance of the surface, and P_r is the transmit power from the r-th LED.

Fig. 2 presents the geometry of a multipath VLC channel with an object located in the room. It should be noted that lights may arrive from multiple paths (i.e., LoS, reflected), which are defined as:

$$L_0 = \frac{A_{PD}(m+1)\cos^m\phi_0^1\cos\theta_0^1}{2\pi d_0^2}, \tag{4}$$

$$L_1 = \frac{A_{eff}(m+1)\cos^m\phi_0^3\cos\theta_0^3}{2\pi d_1^2}, \tag{5}$$

$$L_2 = \frac{A_{PD}\cos^m\cos\phi_1^3 cos\theta_1^3}{\pi d_2^2}, \tag{6}$$

$$L_3 = \frac{A_{eff}(m+1)\cos^m\phi_0^2\cos\theta_0^2}{2\pi d_3^2}, \tag{7}$$

$$L_4 = \frac{A_{PD}\cos^m\cos\phi_1^2 cos\theta_1^2}{\pi d_4^2} \tag{8}$$

The channel impulse responses are then give by:

$$h^0(t_1; LED) = L_0 P\mathbb{1}\left[\frac{\theta_0^1}{FoV}\right]\delta\left(t - \frac{d_0}{c}\right), \tag{9}$$

$$h_1^1(t_2; LED) = \int_S L_1 L_2 \Gamma^1 \mathbb{1}\left[\frac{\theta_1^3}{FoV}\right]\delta\left(t - \frac{d_1+d_2}{c}\right)\mathrm{d}A_{eff}, \tag{10}$$

$$h_2^1(t_2; LED) = \int_S L_3 L_4 \Gamma^1 \mathbb{1}\left[\frac{\theta_1^2}{FoV}\right]\delta\left(t - \frac{d_3+d_4}{c}\right)\mathrm{d}A_{eff} \tag{11}$$

TABLE I: Simulation parameters

Parameter	Value
Reflection coefficient	0.48
Area of the reflecting element	0.01 m^2
Transmit power	1 w
The semi-angle of half power of the LED	60 degree
Field of view (FoV)	90 degree
Rx's effective area	1 cm^2

Once the ray tracing model has been described, we can proceed to present the algorithm. For every pair Tx-Rx the system is calibrated measuring the ray tracing of the light without the object. Then, an object is placed and for every pair Tx-Rx, we measure again the ray tracing. With all these information, the system can determine the shape of the object by analyzing which rays are obstructed. For each traced ray, we determine the ray's arrival time and its trajectory in order to check if the object could be detected at the Rx. Table I shows the key simulation parameters adopted in this work for ray tracing in an indoor environment. In simulation, we consider only LoS paths and/or NLoS paths with a single reflection, since contributions from higher order reflections are considered negligible. However, in experimental investigation only rays received via LoS paths are considered.

B. Shape detection

The shape detection is performed out by comparing a set of rays that reach the Rx with and without an object within the room. The Li-Tect was calibrated with a room with furniture without considering the blocked paths. Note that, higher accuracy can be achieved if the object is detected in a space where there are a large number of unblocked paths.

Monitoring the indoor environment and shape detection is carried out by finding the intersection points between rays in presence of an object located in the room. In computing the number of intersections, there is a trade-off between the complexity and measurement accuracy. In the worst-case scenario, Li-Tect will compute all intersections between the existing rays whose angles of arrival diverge the least from rays blocked by the object. To improve accuracy of the object contour's detection we carried out the followings: (i) compute all possible intersections between rays, which are collected at the Rx, and filter the corresponding output to determine the voids left behind by the intersection points in an area where the object is present[1]; (ii) take a set of intersection points and use them as the triangle vertices to derive a 3D Delaunay triangulation; (iii) consider all triangles with circumscribed circle radius exceeding the user-defined threshold of 50 cm; and (iv) estimate the shape of the object from the alpha-shape of the set of all vertices of these triangles.

Fig. 3 shows a block diagram for shape detection procedure which includes calculation of circumcircles, triangles, determining the free boundary facets of the triangulation and detecting the alpha shape from the determined intersection

[1]We remark that the departure angles tested by the ray tracer belong to a discrete set, hence it is not granted that two rays will intersect perfectly in a 3D environment. Therefore, we consider the minimum distance among rays and declare that an intersection exists if such distance is below a threshold.

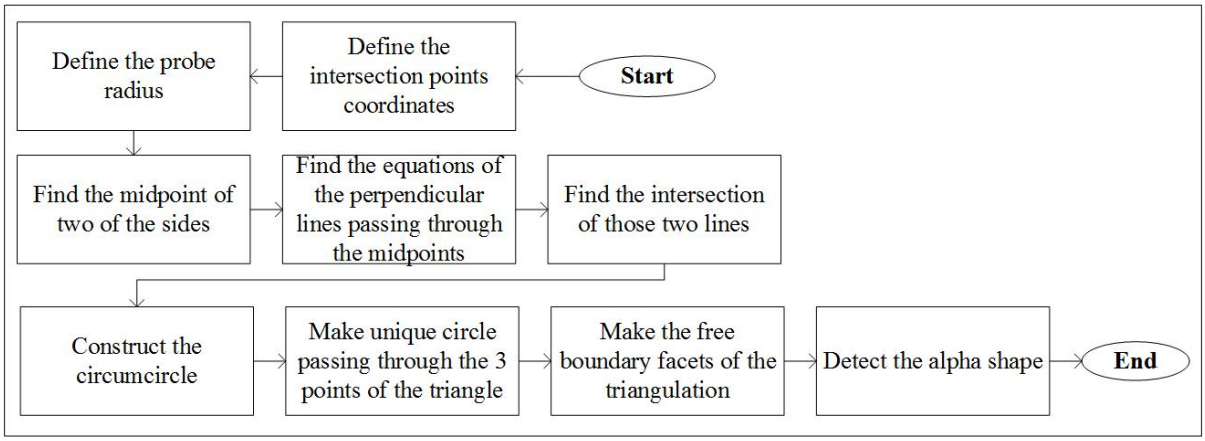

Fig. 3: The shape detection procedure.

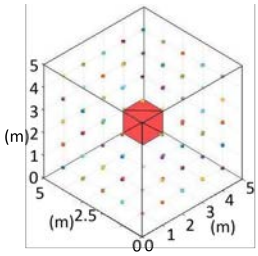

Fig. 4: Shape of a cubic object detected using LoS rays. The dots on the walls represent VLSs.

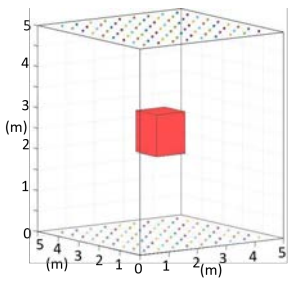

(a) Scenario with VLSs on.

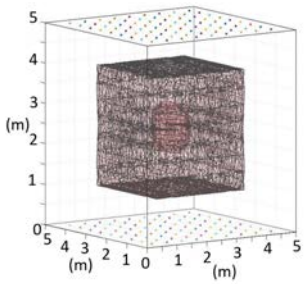

(b) Mesh obtained from LOS path from the opposite walls in a room.

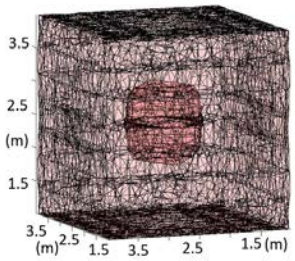

(c) Close-up view of (b) clearly showing the detected shape.

Fig. 5: Detection of a cubic object via VLSs placed on floor and ceiling.

points. The baseline version of Li-Tect works based only on the LoS paths. However, rays reflected by the object and room surfaces within the network area can also be used, because the power contribution is relatively high and thus, they can be detected. In the following section, we present the generated results for both cases.

IV. Simulation Results

Simulations have been carried out for different indoor scenarios - represented by a rectangular shape room of different sizes - with a number of VLSs distributed in different topologies and using Matlab. Without loss of generality, we assumed that, VLSs can be considered as Txs and Rxs.

A. Detecting a cubic object

As proof of concept for Li-Tect, we consider detection of a cubic object located at the center of a room of size $5\times5\times5$ m^3, as shown in Fig. 4. We consider 96 VLSs uniformly distributed at the six sides of the room (i.e., 16 per side) with 1 m spacing between nodes. Taking the collected trajectories into account, we detect the blocked rays among all LoS and the first reflection paths. Subsequently, Li-Tect finds the intersection points among the remaining rays in the presence of the object. Finally, the points are collected and subsequently the shape of the object is detected using the inverse convex hull function, that works by finding the inner hull of a set of collected points.

B. Detecting a cube with smart lights placed on the opposite sides of a room

Here, we now consider the same scenario as before except for VLSs being located on the two opposite sides of the room. In this configurations, it is more challenging to detect the sides of the object by using only LoS rays. Thus, we need to increase the number of LEDs in order to improve the accuracy of the measurement. Therefore, keeping the same arrangement for the object as in Fig. 4, we have used two 9×9 grids (a total of 162 nodes) on the floor and the ceiling, see Fig. 5a). Fig. 5b shows the mesh pattern generated by the Delaunay triangulation method based on the intersections between the not blocked rays by the cubic object. The close-up view of the mesh with the object is depicted in Fig. 5c. In both figures, the

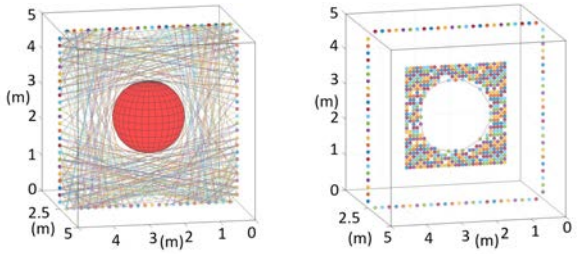

(a) LoS rays around a sphere. (b) Shape detection, LoS rays.

Fig. 6: Sphere section estimate.

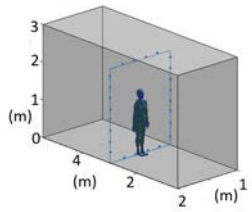

Fig. 7: Scenario for the detection of a human figure.

inner mesh (colored in a darker shade of red) corresponds to the estimated shape of the object, which adheres quite closely to the actual shape of the cube. The slightly more rounded sides of the estimated shape are due to the deployment of nodes only on the floor and the ceiling, which makes difficult to determine the boundaries of the sides of the cube.

C. Detecting a spherical object

Next, we consider the detection of a spherical object located within a room. For the detection of the circular shape of the object using Li-Tect, we have deployed 96 VLSs with a square topology in order to cover a room section as it is shown in Fig. 6a. Considering the LoS rays that are not blocked by the sphere, we obtain the intersection points as illustrated in Fig. 6b, where the Delaunay triangulation is not shown for clarity purposes. Note that, resulting shape of the object reveals a good approximation of a circular section, as expected.

D. Detecting a human figure

Fig. 7 show 24 VLSs in a rectangular shape i.e., 4- and 8-nodes on top and bottom and two sides, respectively, which resembles a door frame. A human body modeled in 3D as in [25] is placed in the center of the frame. Similar to the scenarios outlined above, Li-Tect is calibrated with rays in a room with no shadowing or blocking, which is used as a reference to compare with un-blocked rays by the human body in order to estimate its shape. Unlike in the previous simpler scenarios, here we consider also rays as a result of single reflections, either on the room boundaries or on the human figure. Using LiTect's estimation, the human figure shape detections are depicted in Fig. 8 for both LoS and LoS with reflections paths. For LoS, see Fig. 8a, considering the low number of VLSs employed, the estimated shape - showing the height (1.7 m) and main outline - closely resembles the human figure as in Fig. 7, which is sufficient for identifying a

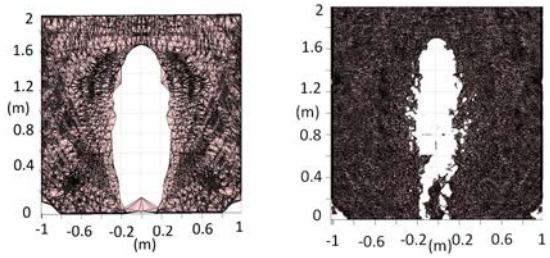

(a) Only LoS rays. (b) LoS and reflected rays.

Fig. 8: Detection of the shape of the section of a human figure passing through a door.

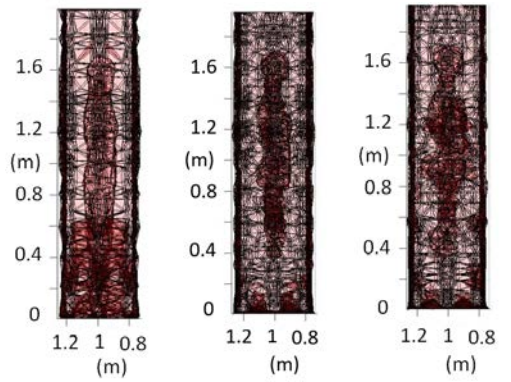

(a) LoS rays. (b) LoS and reflected rays. (c) Only reflected rays.

Fig. 9: 3D shape detection using different type of rays.

person in certain applications. Considering the first reflection the estimated shape is shown in Fig. 8b, which outlines additional details including the legs and possibly the arms.

Finally, we consider the detection of the human shape using a 3D configuration where the VLSs are arranged into 3 rectangular topologies as in Fig. 7, with a spacing of 20 cm between the nodes. The results are shown in Fig. 9 for LoS, LoS with reflections, and reflections only. It should be highlight here that, figures are shown from the side for enhanced visualization. Fig. 9a shows sufficiently details of the human shape including the chest, which is slightly larger than the waist. Factoring of the reflected rays help to further increase the resolution of the human figure's contour, this way it is possible to distinguish additional details including e.g., the shape of the neck. It should be noted that, the reflected rays are the only way to detect the most concave parts of an object, hence they typically allow the estimated shape to follow the contour of the actual shape more closely, as it can be seen in Fig. 9b and Fig. 9c.

V. Practical Experiment Results

The proposed Li-Tect system is experimentally implemented into a prototype in order to validate its performance. We have chosen a scenario where we can evaluate shape detection of an object in two and three dimensions where Tx/Rx nodes are located within door frame in one and two rows as it is shown in Fig. 7. The flow chart for experimental setup is shown in

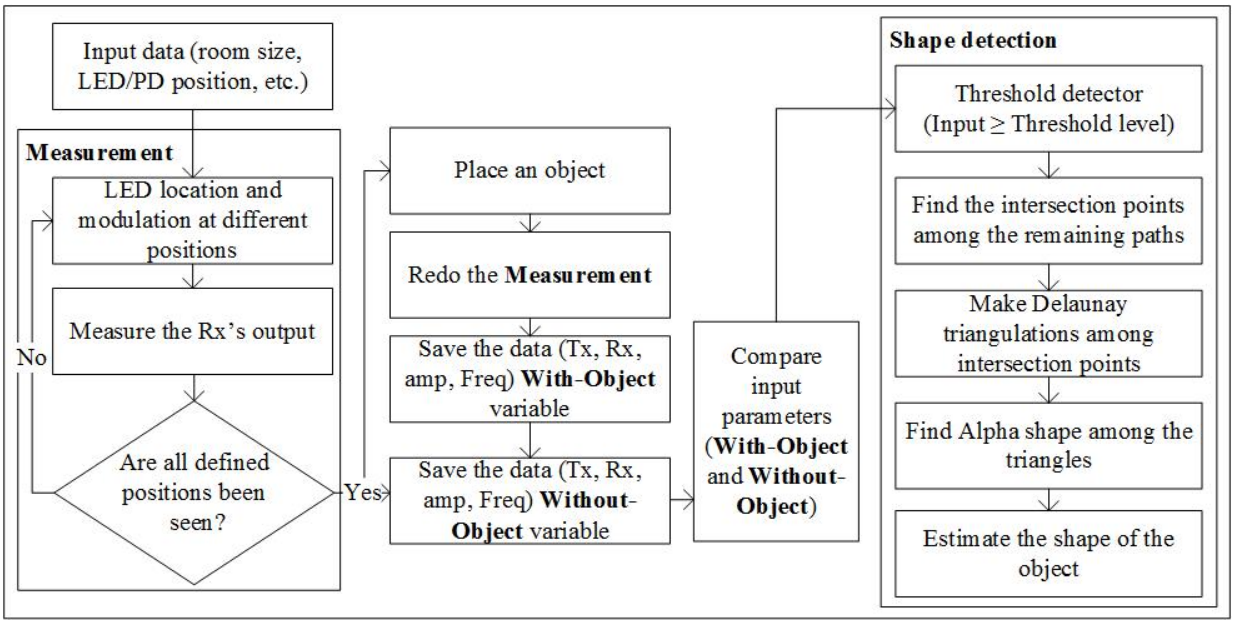

Fig. 10: Experimental setup flow chart.

Fig. 10, whereas the experimental system block diagram is shown in Fig. 11. We implement the same topology designed for human detection both in 2D and 3D as it was outlined in the previous sections. The structure for placing the VLSs are almost the same, but the type of the object used, the room size, and number of the nodes are changed. We consider a relatively small size of a room, fewer number of Txs with low transmit power, and a typical optical Rx.

We have assumed that each VLS has information on the location and identification of other nodes, and therefore each Rx is able to distinguish multiple received rays arriving from different LoS paths based on their identity number (IN) and the assigned frequency. We have used a cubic shape object, which is covered with white papers, and is located at the center of the room on the floor.

TABLE II: Positions of VLSs in a 2D experimental setup

VLSs positions in the first scenario			
Tx1	(34cm, 57cm, 41cm)	**Rx1**	(34cm, 1cm, 41cm)
Tx2	(34cm, 57cm, 31cm)	**Rx2**	(34cm, 1cm, 31cm)
Tx3	(34cm, 57cm, 21cm)	**Rx3**	(34cm, 1cm, 21cm)
Tx4	(34cm, 57cm, 12cm)	**Rx4**	(34cm, 1cm, 12cm)
Tx5	(34cm, 57cm, 2cm)	**Rx5**	(34cm, 1cm, 2cm)
Tx6	(34cm, 2cm, 56cm)	**Rx6**	(34cm, 2cm, 1cm)
Tx7	(34cm, 19cm, 56cm)	**Rx7**	(34cm, 19cm, 1cm)
Tx8	(34cm, 38cm, 56cm)	**Rx8**	(34cm, 38cm, 1cm)
Tx9	(34cm, 57cm, 56cm)	**Rx9**	(34cm, 57cm, 1cm)

1) 2D based Shape detection: VLSs are placed on sides of the room as outlined in the simulation section. Table II shows the position of each LED and PD within the room. We assign the same transmit power as 100 mw to each LED and different frequencies. However, we only consider rays propagated via LoS and received by the angle of FoV of the Rxs in order to detect the shape of an object within the indoor environment.

We repeat the experiment under the same conditions twice; with and without an object. After collecting the information of propagation paths, we calculate voltage peak-to-peak (Vpp) on each Rx side. Based on the calculation results and due to frequency-division application, we determine the blocked rays and obtain the information for the existing rays for further processing using Li-Tect. After finding the intersection points among the existing rays and applying the inverse concave hull method on achieved vertices, we detect the shape boundaries of the object located within the room in 2D.

TABLE III: Positions of VLSs in a 3D experimental setup

VLSs positions in the second scenario			
Tx1	(28cm, 57cm, 41cm)	**Rx1**	(28cm, 1cm, 41cm)
Tx2	(42cm, 57cm, 41cm)	**Rx2**	(42cm, 1cm, 41cm)
Tx3	(28cm, 57cm, 31cm)	**Rx3**	(28cm, 1cm, 31cm)
Tx4	(42cm, 57cm, 31cm)	**Rx4**	(42cm, 1cm, 31cm)
Tx5	(28cm, 57cm, 21cm)	**Rx5**	(28cm, 1cm, 21cm)
Tx6	(42cm, 57cm, 21cm)	**Rx6**	(42cm, 1cm, 21cm)
Tx7	(28cm, 57cm, 12cm)	**Rx7**	(28cm, 1cm, 12cm)
Tx8	(42cm, 57cm, 12cm)	**Rx8**	(42cm, 1cm, 12cm)
Tx9	(28cm, 57cm, 2cm)	**Rx9**	(28cm, 1cm, 2cm)
Tx10	(42cm, 57cm, 2cm)	**Rx10**	(42cm, 1cm, 2cm)
Tx11	(28cm, 2cm, 56cm)	**Rx11**	(28cm, 2cm, 1cm)
Tx12	(42cm, 2cm, 56cm)	**Rx12**	(42cm, 2cm, 1cm)
Tx13	(28cm, 19cm, 56cm)	**Rx13**	(28cm, 19cm, 1cm)
Tx14	(42cm, 19cm, 56cm)	**Rx14**	(42cm, 19cm, 1cm)
Tx15	(28cm, 38cm, 56cm)	**Rx15**	(28cm, 38cm, 1cm)
Tx16	(42cm, 38cm, 56cm)	**Rx16**	(42cm, 38cm, 1cm)
Tx17	(28cm, 57cm, 56cm)	**Rx17**	(28cm, 57cm, 1cm)
Tx18	(42cm, 57cm, 56cm)	**Rx18**	(42cm, 57cm, 1cm)

2) Shape detection in 3D: Here, we aim to present the functionality of Li-Tect algorithm in 3D detection of the shape of an object within the indoor. In this scenario, we place LEDs on two rectangular sections lined up at a distance of 14 cm from each other. We multiply the number of VLSs by two in order to detect the shape of an object in 3D. Table III shows the positions of LEDs and PDs distributed on room surfaces.

TABLE IV: Experiments parameters

Room size	68 cm x 58 cm x 57 cm
Object size	15 cm x 10 cm x 30 cm
LED:	
Semi-angle of half power	60 degree
Transmit power	150 mw
Bandwidth	< 5 MHz
PD:	
Field of view	90 degree
Wavelength range	350 - 1000 nm
Bandwidth	100 MHz
Responsivity	< 0.44 A/W
Effective area	13 mm^2

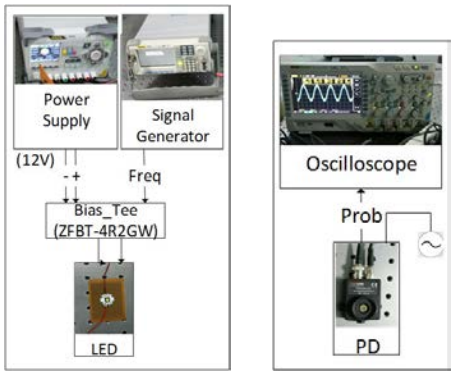

(a) (b)

Fig. 11: Experimental system diagram: (a) transmitter, and (b) receiver.

As in the first scenario, we apply frequency-division method in order to emit the light and consider the LEDs transmission power equal to each other. After gathering the achieved information regarding each propagation path received by each Rxs in two phases; with and without the presence of an object. Then, we calculate the intersection points among the existing paths after the object is in the room and detect the shape of an object applying 3D Delaunay triangulation and the alpha-shape method on the set of points. Table IV presents the key parameters used in experiments.

A. Experiment results

As it was explained before, the signal amplitude is used in our prototype to detect which LoS path is blocked by an object in the room. Here, we present a work sample revealing the blocked paths once an object appears within the room. Note, we observed no differences between the received signals in both phases, thus indicating that there is no obstacle in that area to block LoS paths. However, Fig. 12 presents five signals with different frequencies (distinguished by different colors) transmitted by the first five Txs mentioned in Table II and received by the Rx located at 34, 1 and 12 cm. As shown, Vpp is reduced from 0.02 V to 0.004 V due to blocking by the object.

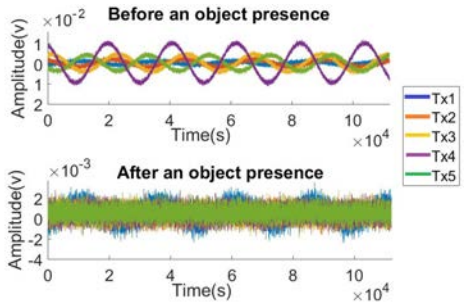

Fig. 12: Measured signal amplitude at the receiver, before and after an object being located.

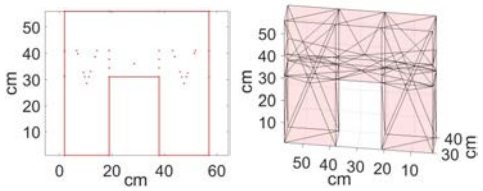

(a) 2D shape detection. (b) 3D shape detection.

Fig. 13: Experimentally generated shape detection using Li-Tect.

B. Shape detection using Li-Tect

As it is revealed in Fig. 13a, there are several points in red color, which present the intersection points among the remaining paths in the presence of an object in the room. After applying Li-Tect algorithm on the acquired data in practical experiment, and using the inverse concave hull, an accurate shape of a rectangle is obtained for the inner side of the larger area. The actual length of the object used in the experiment is 15 cm, however our result shows that the estimated length of the object is 19 cm and its height is almost the real object. The reason behind the small error in the length is due to the arrangement of Txs and Rxs positions within the room. Therefore, there is a trade-off between the number of VLSs and accuracy of the object size estimation using Li-Tect. However, it worth mentioning that, the most significant function of this algorithm is in detecting the shape and posture of an object in two and three dimensions using comparatively less number of VLSs. Moreover, in our simulation investigations, we have shown how the accuracy of the shape detection of an object improves using not only the LoS paths but also the first reflections.

C. shape detection using Li-Tect

Finally the Fig. 13b reveals the 3D shape detection results using Li-Tect algorithm in practical experiment. Note that, in this figure we have not showed the intersection points in order to avoid complexity. As the figure shows, there is a 3D mesh in the shape of triangles connecting the intersection points among the remaining LoS paths achieved by the practical experiment, to each other with inclusion of an object. The inner vertices of the polygon mesh reveals the boundary of

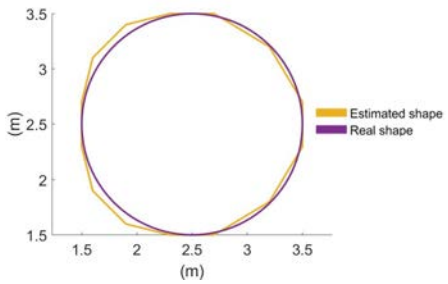

Fig. 14: 2D comparison of the real shape and estimated shape of the object using Li-Tect in the simulation.

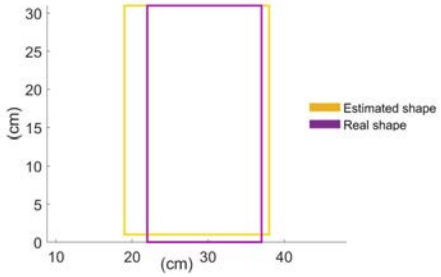

Fig. 15: 2D comparison of the real shape and estimated shape of the object using the experimental Li-Tect test-bed.

the object, if it exists at all. The figure estimates the size of an object with a length of 17 cm, a width 10 cm and a height 30 cm, which are more accurate in comparison with the 2D shape detection scenario. This is because of employing a relatively higher number of VLSs and on the 3D arrangement of the devices within the indoor environment.

D. Mean Squared Error calculation in 2D detection experiments

TABLE V: Mean Squared Error

Experiment type	LEDs quantity	Shape of object	MSE
Practical	9	cube	5.50
Simulation	96	sphere	0.0567

Next we compared both simulated and measured shape estimated results achieved by Li-Tect and the real shape of the object to evaluate the functionality of the proposed algorithm in order to detect object's shape. Moreover, we have used only the 2D detection scheme, which are easier to demonstrate in figures. Fig. 14 demonstrates the comparison between the Li-Tect estimated shape using simulations (Fig. 6) and the real shape of the object. As the figure shows, the estimation results are quite close to the real shape of the object.

Finally, Fig. 15 shows 2D comparison of real and estimated shapes of the object using Li-Tect experiment as in Fig. 13a.

We have calculated the mean squared error (MSE) for both practical and simulation results. For this case, the MSE depends on the number of the Txs, the transmit power, the position of the Rxs and the level of shape complexity of the object. As shown in Table V, for higher number of Txs the MSE is lower. The reason behind is because we collect more information regarding the propagation path. Therefore, we achieve more intersection points among the remaining paths in the presence of an object, which leads to more accurate detection of the shape of an object within the environment as expected.

VI. Conclusions

This paper presented Li-Tect algorithm to passively estimate the 3D shape of objects using VLSs within an indoor environment. To perform the estimation, Li-Tect detected light paths that were blocked by an object and compared them with a set of paths with no object. Li-Tect achieved a significant improved shape estimation accuracy only using the information provided by line-of-sight paths. The typically convex contours obtained in this case can be enriched by including the reflected paths, which provided additional details on the object's shape including the concave sections whose detection is typically precluded by the processing of LoS paths.

We presented both simulation and experiments results demonstrating the functionality of Li-Tect in 2D and 3D shape estimation in an indoor environment. By means of simulation, we considered different environment topologies, varying number of VLSs and various levels of shape complexity of the object to asses the flexibility and power of Li-Tect algorithm. Besides, we implemented the algorithm in prototype using only VLSs with no additional equipment such as sensors and cameras. We showed that, the accuracy of the object's shape detection depended on the number of VLSs and their position distribution within the experimental environment. We have showed that considering reflected propagation paths led to a more accurate detection of the shape, although complexity increases.

Future work will include implementation of Li-Tect in a room with reflective surfaces and an object made of reflective material using more sensitive photodiods such as avalanche photodiodes and LEDs with higher transmit power levels.

VII. Acknowledgments

This work was supported in part by the Spanish Government under the National projects 'ELISA' and 'TERESA-ADA' with ID TEC2014-59255-C3-3-R and TEC2017-90093-C3-2-R, respectively.

References

[1] Z. Ghassemlooy, L. N. Alves, S. Zvanovec, and M.-A. Khalighi, *Visible Light Communications: Theory and Applications*. CRC Press, 2017.

[2] F. Miramirkhani and M. Uysal, "Channel modeling and characterization for visible light communications," *IEEE Photonics Journal*, vol. 7, no. 6, pp. 1–16, 2015.

[3] P. Luo, Z. Ghassemlooy, H. Le Minh, E. Bentley, A. Burton, and X. Tang, "Fundamental analysis of a car to car visible light communication system," in *Communication Systems, Networks & Digital Signal Processing (CSNDSP), 2014 9th International Symposium on*. IEEE, 2014, pp. 1011–1016.

[4] D. Marinos, C. Aidinis, N. Schmitt, J. Klaue, J. Schalk, T. Pistner, and P. Kouros, "Wireless optical ofdm implementation for aircraft cabin communication links," in *Wireless Pervasive Computing (ISWPC), 2010 5th IEEE International Symposium on*. IEEE, 2010, pp. 465–470.

[5] S. Ahamed, "Visible light communication in railways," 2016.

[6] P. Singh, G. Singh, and A. Singh, "Implementing visible light communication in intelligent traffic management to resolve traffic logjams."

[7] Z. Ghassemlooy, W. Popoola, and S. Rajbhandari, *Optical wireless communications*. CRC Press Boca Raton, FL, 2012.

[8] B. Lin, X. Tang, Y. Li, M. Zhang, C. Lin, Z. Ghassemlooy, Y. Wei, Y. Wu, and H. Li, "Experimental demonstration of optical camera communications based indoor visible light positioning system," *A A*, vol. 2, p. 2.

[9] A. Sewaiwar, S. V. Tiwari, and Y.-H. Chung, "Visible light communication based motion detection," *Opt. Express*, vol. 23, no. 14, pp. 18 769–18 776, Jul 2015. [Online]. Available: http://www.opticsexpress.org/abstract.cfm?URI=oe-23-14-18769

[10] Y. Yang, J. Hao, J. Luo, and S. J. Pan, "Ceilingsee: Device-free occupancy inference through lighting infrastructure based led sensing," in *2017 IEEE International Conference on Pervasive Computing and Communications (PerCom)*, March 2017, pp. 247–256.

[11] D. Wu, W. D. Zhong, Z. Ghassemlooy, and C. Chen, "Short-range visible light ranging and detecting system using illumination light emitting diodes," *IET Optoelectronics*, vol. 10, no. 3, pp. 94–99, 2016.

[12] A. Mostafa and L. Lampe, "Physical-layer security for indoor visible light communications," in *Communications (ICC), 2014 IEEE International Conference on*. IEEE, 2014, pp. 3342–3347.

[13] S. Schmid, G. Corbellini, S. Mangold, and T. R. Gross, "Led-to-led visible light communication networks," in *Proceedings of the fourteenth ACM international symposium on Mobile ad hoc networking and computing*. ACM, 2013, pp. 1–10.

[14] A. Burton, H. L. Minh, Z. Ghasemlooy, and S. Rajbhandari, "A study of led lumination uniformity with mobility for visible light communications," in *2012 International Workshop on Optical Wireless Communications (IWOW)*, Oct 2012, pp. 1–3.

[15] B. G. Guzman, A. A. Dowhuszko, V. P. G. Jimenez, and A. I. Perez-Neira, "Robust cooperative multicarrier transmission scheme for optical wireless cellular networks," *IEEE Photonics Technology Letters*, vol. 30, no. 2, pp. 197–200, Jan 2018.

[16] B. G. Guzman and V. P. G. Jimenez, "Dco-ofdm signals with derated power for visible light communications using an optimized adaptive network-based fuzzy inference system," *IEEE Transactions on Communications*, vol. 65, no. 10, pp. 4371–4381, Oct 2017.

[17] W. A. Cahyadi, Y.-H. Kim, Y.-H. Chung, and Z. Ghassemlooy, "Efficient road surface detection using visible light communication," in *Ubiquitous and Future Networks (ICUFN), 2015 Seventh International Conference on*. IEEE, 2015, pp. 61–63.

[18] P. Luo, M. Zhang, Z. Ghassemlooy, H. Le Minh, H.-M. Tsai, X. Tang, and D. Han, "Experimental demonstration of a 1024-qam optical camera communication system," *IEEE Photon. Technol. Lett.*, vol. 28, no. 2, pp. 139–142, 2016.

[19] T. Li, C. An, Z. Tian, A. T. Campbell, and X. Zhou, "Human sensing using visible light communication," in *Proceedings of the 21st Annual International Conference on Mobile Computing and Networking*. ACM, 2015, pp. 331–344.

[20] T. Li, Q. Liu, and X. Zhou, "Practical human sensing in the light," in *Proceedings of the 14th Annual International Conference on Mobile Systems, Applications, and Services*. ACM, 2016, pp. 71–84.

[21] F. Adib, C.-Y. Hsu, H. Mao, D. Katabi, and F. Durand, "Capturing the human figure through a wall," *ACM Transactions on Graphics (TOG)*, vol. 34, no. 6, p. 219, 2015.

[22] L. Gong, W. Yang, D. Man, G. Dong, M. Yu, and J. Lv, "Wifi-based real-time calibration-free passive human motion detection," *Sensors*, vol. 15, no. 12, pp. 32 213–32 229, 2015.

[23] B. Mrazovac, M. Z. Bjelica, D. Kukolj, S. Vukosavljev, and B. M. Todorovic, "System design for passive human detection using principal components of the signal strength space," in *Engineering of Computer Based Systems (ECBS), 2012 IEEE 19th International Conference and Workshops on*. IEEE, 2012, pp. 164–172.

[24] K. Lee, H. Park, and J. R. Barry, "Indoor channel characteristics for visible light communications," *IEEE Communications Letters*, vol. 15, no. 2, pp. 217–219, 2011.

[25] (2017, May). [Online]. Available: https://es.mathworks.com/matlabcentral/fileexchange/236-nancy-body-m